

Identification of Post-necking Tensile Stress–Strain Behavior of Steel Sheet: An Experimental Investigation Using Digital Image Correlation Technique

Surajit Kumar Paul, Satish Roy, S. Sivaprasad, H.N. Bar, and S. Tarafder

(Submitted October 18, 2017; in revised form February 7, 2018; published online October 19, 2018)

The stress–strain behavior of sheet metal is commonly evaluated by tensile test. However, the true stress–strain curve is restricted up to uniform elongation of the material. Usually, after the uniform elongation of the material the true stress–strain is obtained by extrapolation. The present work demonstrates a procedure to find out the true tensile stress–strain curve of the steel sheet after necking using digital image correlation (DIC) technique. Hill's normal anisotropic yield criteria and local strains measured by DIC technique are used to correct the local stress and strain states at the diffuse necked area. The proposed procedure is shown to successfully determine the true tensile stress–strain curve of ferritic and dual-phase steel sheets after necking/uniform elongation.

Keywords diffuse necking, digital image correlation, post-necking tensile stress–strain curve, sheet metal, tensile test

1. Introduction

Finite element method has been extensively used nowadays to optimize metal forming operations, simulation of crash events and other large deformation processes. Many metal forming operations lead to strains that are beyond the uniform elongation of the material. For a precise simulation of crash events and machining operations, information on stress–strain response of materials over a large range of strain is mandatory. Therefore, there is a requirement of generation of stress–strain response of a material beyond its uniform elongation. The classical methods of obtaining stress–strain behavior of a material such as conventional tensile tests are not sufficient to get the stress–strain response after necking (Ref 1). More expensive and cumbersome hydraulic bulge tests are normally used to obtain the required stress–strain information in such cases (Ref 2). Of late, few research groups (Ref 3–10) have worked on hybrid methods, employing a combination of experiment, analysis and finite element simulation, to construct post-necking tensile stress–strain curve. However, these methods are not simple and straightforward to employ in an engineering scenario.

Bridgman (Ref 11) was the first to propose a method for determining the post-necking hardening behavior of a round bar. Principally, the proposal was to correct the geometry of necking profile (i.e., local area correction). Zhang et al. (Ref 12) extended this concept for a tensile test specimen with cross

section of rectangular geometry. However, this method is valid only up to a maximum aspect ratio of 8 for the rectangular cross section. Koc and Stok [13] proposed an inverse method based on the experimentally measured tensile forces. Kajberg and Lindkvist (Ref 14) combined the in-plane displacement fields measured by digital speckle photography (DSP) and inverse modeling, to describe the stress–strain response of a sheet metal at high plastic strains. Tao et al. (Ref 15) reported an iterative procedure to determine the stress–strain curve beyond necking using digital image correlation (DIC). Holmberg et al. (Ref 16) employed tensile tests using DIC to determine the formability of sheet metal. Merklein et al. (Ref 17) determined the thermo-mechanical material characteristics by measuring deformation of tensile specimens using DIC. Grédiac and Pierron (Ref 18) successfully determined the post-necking plastic material behavior through DIC and virtual field based inverse modeling. Marth et al. (Ref 10) used optical full-field displacement measurements to compute local strain fields and stress–strain curve of the material after necking. Coppieters et al. (Ref 5) presented an alternative technique without using a finite element (FE) model to identify the hardening behavior of sheet metal after necking. This method minimized the difference between the internal and external work in the necking region in a tensile experiment. Tardif and Kyriakides (Ref 6) predicted post-necking true stress–strain curve of Al-6061-T6 sheet metal. They simulated the tensile test of Al-6061-T6 sheet metal numerically using a 3D finite element model, and the response of the sheet metal was iteratively extrapolated until the simulated and measured force–elongation matched. They also validated their method by measurement of strains in necking zone and geometry of the neck. Gerbig et al. (Ref 9) presented a general framework for coupling DIC with FE analysis to find out material parameters from measurements of non-uniform displacement fields in a tensile specimen. The aim was to reduce the discrepancy between measured and calculated force and displacement fields by continually correcting the material constants in a selected constitutive equation. Wang and Tang (Ref 7) predicted tensile true stress–strain curve after necking from standard flat coupon by numerical simulation with a

Surajit Kumar Paul, Department of Mechanical Engineering, Indian Institute of Technology Patna, Patna, Bihar, India; **Satish Roy**, **S. Sivaprasad**, **H.N. Bar**, and **S. Tarafder**, Fatigue and Fracture Group, CSIR-National Metallurgical Laboratory, Jamshedpur 831007, India. Contact e-mails: paulsurajit@yahoo.co.in, surajit@iitp.ac.in.

multi-linear strain hardening model. Zhao et al. (Ref 8) also presented a method (combination of simple tensile test and FE analyses) for obtaining the stress–strain response of sheet metals over a large strain range.

Determination of post-necking true stress–strain curve can be done in three ways. The first procedure is to correct stress–strain states in the necked region by introduction of a correction factor. Zhang et al. (Ref 12) derived such correction factor from extensive finite element study for a tensile test specimen with rectangular cross section. Researchers reported various such correction factors for tensile test specimens with circular (Ref 11) and rectangular (Ref 12, 19) cross sections. The second procedure is inverse method based on finite element model updating. An anticipated stress–strain curve of the material is supplied into the finite element program, and the simulated load–axial displacement curve is compared with the experimental load–axial displacement curve. The post-necking stress–strain curve is achieved when the difference between experimental and simulated load–axial displacement curves lies within a predefined range (Ref 8, 13, 20, 21). Kim et al. (Ref 21) reported that the selection of a hardening law is vital to obtain the post-necking strain hardening response precisely. In the third procedure, instead of phenomenological hardening laws a piecewise linear hardening model is used (Ref 6, 10, 22). This procedure can describe realistic post-necking stress–strain curve because commonly used hardening laws are unable to describe the stress–strain response properly in some materials, especially at large strains (Ref 6). In all investigations, researchers used DIC to extract neck geometry and validate their procedures. In the present investigation, DIC is used to directly measure correction factor to correct stress–strain states in the necked region.

The finite element-based inverse technique is successfully used by many authors to identify the unknown material parameters of a preselected material model. But, there are some inherent complexities in this FE-based inverse technique. For example, the accuracy depends upon the preselected material model, specimen geometry modeling and finite element model-like type of analysis employed, domain and time discretization used, the boundary conditions applied. Apart from these, the finite element computations are time-consuming and require a certain level of expertise. It is a difficult task to the research community to construct a finite element model which is competent of dealing with the plastic instability effectively. In the present work, an alternative

approach is presented to identify the extended true stress–strain curve after necking/uniform elongation of sheet metal.

2. Experimentation

Cold-rolled commercial ferritic (high strength interstitial free) steel and dual-phase (DP600) steel (contains ferrite and martensite phases) are selected for this investigation. Tensile behavior of DP steel is governed by the volume fraction and morphology (shape, aspect ratio, distribution, etc.) of the martensite, ferrite–martensite interface strength, as well as the grain size and carbon content in the ferrite phase (Ref 23). However, present investigation is limited to the as-received microstructure of DP steel. Sheet thickness of ferritic and DP steels was 1.2 and 1.4 mm, respectively. Flat tensile specimens with a gauge length of 25 mm are used. All specimens are fabricated in such a manner that specimen's loading axis lies in the rolling direction of the sheet. A constant strain rate of 0.001/s is used for conducting the tensile test. All experiments are carried out at laboratory environment in a servo-electric test frame of 35 kN capacity. All tests are continued until fracture of

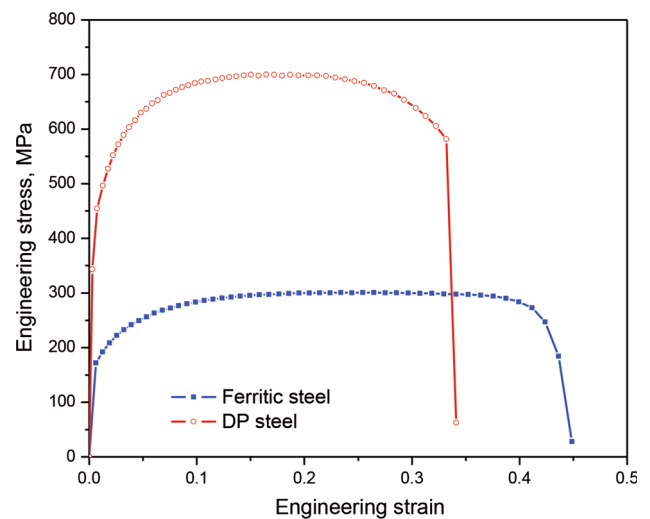


Fig. 2 Tensile stress–strain curve of ferritic and DP steels

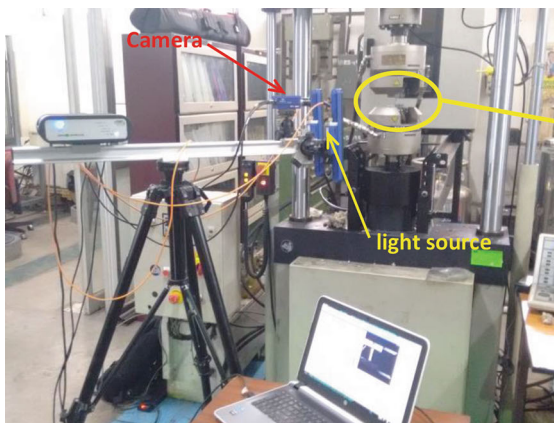
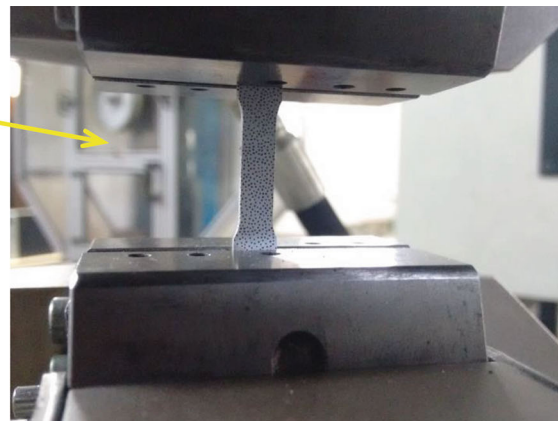


Fig. 1 Servo-electric Instron test frame with LaVision DIC setup for tensile test



the sample. Commercially available 2D DIC system from LaVision (Ref 24) is used for local strain measurement. Tensile test setup with online strain measurement unit is shown in Fig. 1. Speckle pattern foil, supplied by LaVision, is used on one side of the sample. Normally, 100–200 images per test specimen are stored for determination of local strain components.

3. Results and Discussion

Tensile stress–strain curves of ferritic and DP steels are illustrated in Fig. 2. Contours of local strain components, parallel to the loading direction (ϵ_{YY}) and perpendicular to loading direction (ϵ_{XX}) at various overall strain levels during tensile test of a ferritic steel, are shown in Fig. 3 and 4, respectively. A vertical line is selected (Fig. 5) in the middle of the specimen gauge length for investigation of evolution of local strain components at various overall tensile strain levels. The vertical line is drawn through DaVis software supplied by LaVision (Ref 24) for further analysis. Evolution of local strain components (ϵ_{YY} and ϵ_{XX}) along chosen vertical line at various overall strain levels is shown in Fig. 6(a) and (b). The plastic deformation is noted to be homogeneous within the gauge length of the sample up to uniform elongation of the material, after that the deformation is concentrated to a local region. This localization of plastic deformation is normally known as necking. Tardif and Kyriakides (Ref 6) also reported similar type of localization in Al-6061-T6 sheet metal by showing edge profile in the necked area. Necking of a sheet metal can be

classified into two categories such as diffuse and local necking. Normally, diffuse necking is followed by local necking. Strain concentrations in both the width and thickness directions are comparable in the diffuse necking. While, the strain contraction in the thickness direction is far higher than in width direction for local necking (i.e., an indication of plane strain deformation).

For detailed analysis, two horizontal lines (Fig. 7), one at the necked region and the other outside the necked zone but within the gauge length, are selected for investigation of evolution of local strain components (ϵ_{XX} and ϵ_{YY}) at various overall tensile strain levels. Evolution of local strain component (ϵ_{YY}) at necked zone in various overall strain levels is shown in Fig. 8. The variation of the strain component (ϵ_{YY}) across the width of the sample is noted to be small. Therefore, local average strain components (ϵ_{XX} and ϵ_{YY}) at various overall strain levels at the two zones defined earlier (at necked and outside the necked zone) are computed from DIC results. Evolution of this local average strain components (ϵ_{XX} and ϵ_{YY}) in the two zones at various overall strain levels are plotted in Fig. 9(a) and (b). Local average strain components (both ϵ_{XX} and ϵ_{YY}) at outside the necked zone remain almost constant after uniform elongation. On the other hand, the local average strain components within the necked zone increase with the overall strain even after uniform elongation. At the end (last four points), the strain component (ϵ_{XX}) in necked zone remains constant almost up to the fracture event, while ϵ_{YY} increases with straining (Fig. 9a). This indicates that the axial elongation takes place at the expense of thinning (thickness strain) implying a plane strain deformation. Normally, plane strain deformation would occur during local necking. Therefore, local

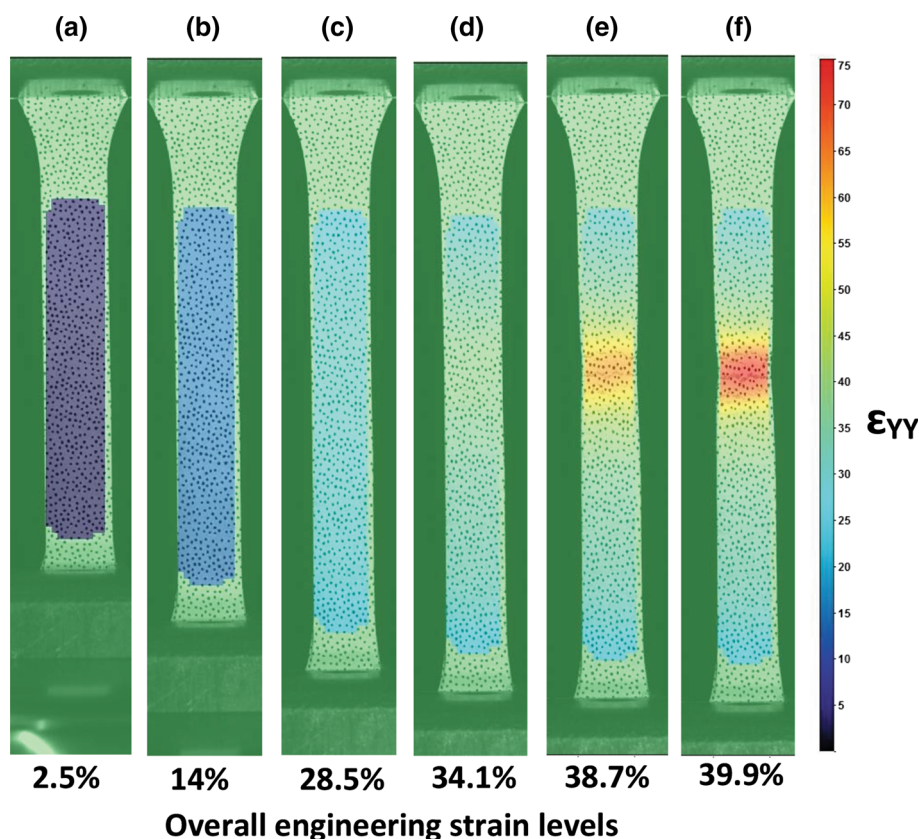


Fig. 3 Contour of local strain component parallel to loading direction (ϵ_{YY}) at various overall strain levels during tensile test of a ferritic steel

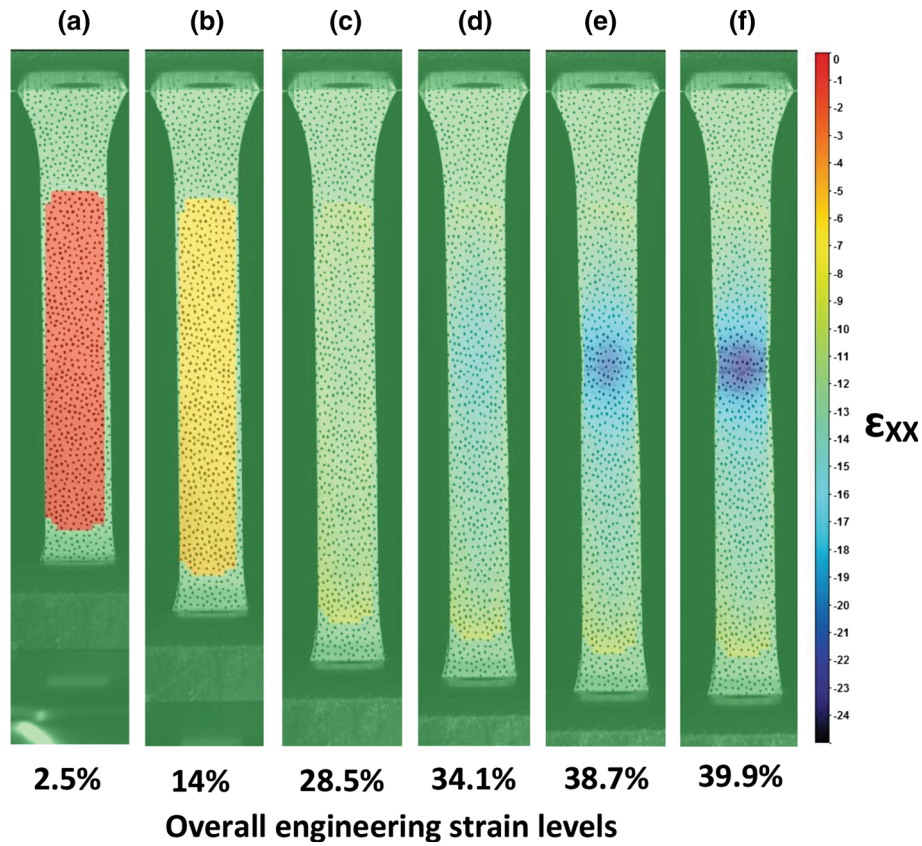


Fig. 4 Contour of local strain component perpendicular to loading direction (ϵ_{XX}) at various overall strain levels during tensile test of a ferritic steel

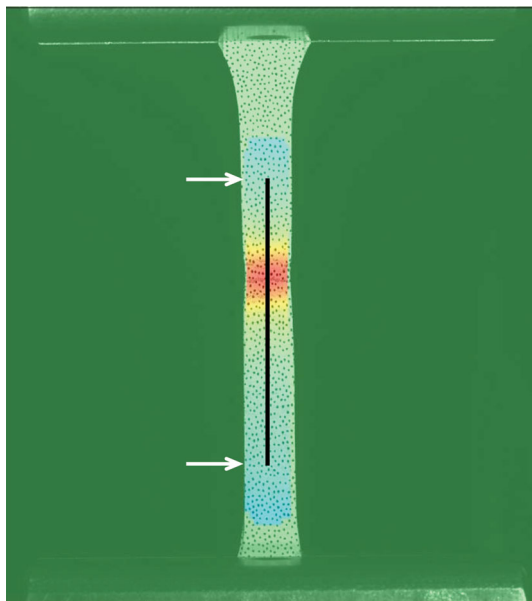


Fig. 5 Vertical line on the middle of the sample surface and within the gauge length for investigation of evolution of local strain components at various overall tensile strain levels

necking is distinguishable for ferritic steel. However, the local necking is not distinguishable for DP steel in Fig. 9(b).

Based on the above observations, a procedure is developed to determine post-necking true stress–strain curve of sheet

metal using a DIC-based local strain measurement, and correction of local stress and strain states. Due to the use of DIC, measurement of local strains in necked region was straightforward and precise. The procedure assumed void formation during diffuse necking will not significantly contribute to the volume change, and thus the volume remains constant in the necked region. The rationale for this assumption is due to the experimental evidence provided by Tasan et al. (Ref 25) who showed through high-resolution SEM and 3D x-ray tomography that the void volume fraction in DP 600 is steel less than 2%. It is thus anticipated that such a low volume fraction of voids would not contribute significantly to the volume change during diffuse necking. It may also be noted that such an assumption is valid only in the cases of diffused necking wherein the necking is very shallow. For the case of localized necking, volume fraction of voids can be high enough and volume constant condition is no longer applicable. Therefore, this procedure cannot be applicable for localized necking. The procedure for determining the post-necking stress–strain curve is as given below:

The strain rate ratio (β) is the ratio of minor strain rate ($d\epsilon_{XX}$) and major strain rate ($d\epsilon_{YY}$) and defined as

$$\beta = \frac{d\epsilon_{XX}}{d\epsilon_{YY}} \quad (\text{Eq 1})$$

Similarly, the stress ratio (α) is the ratio of minor stress (σ_{XX}) and major stress (σ_{YY}) and defined as

$$\alpha = \frac{\sigma_{XX}}{\sigma_{YY}} \quad (\text{Eq 2})$$

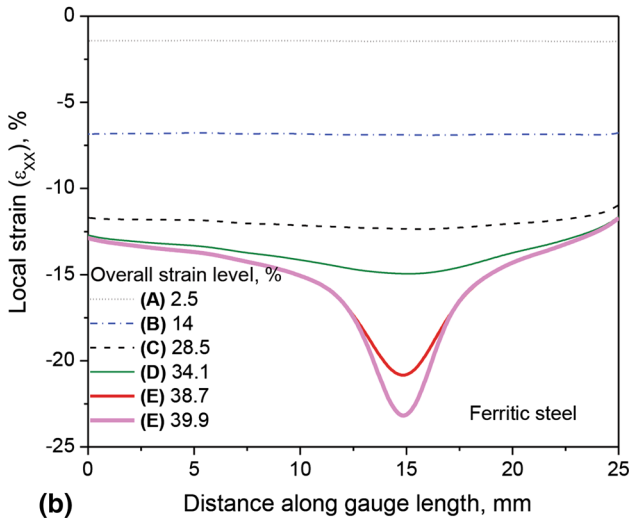
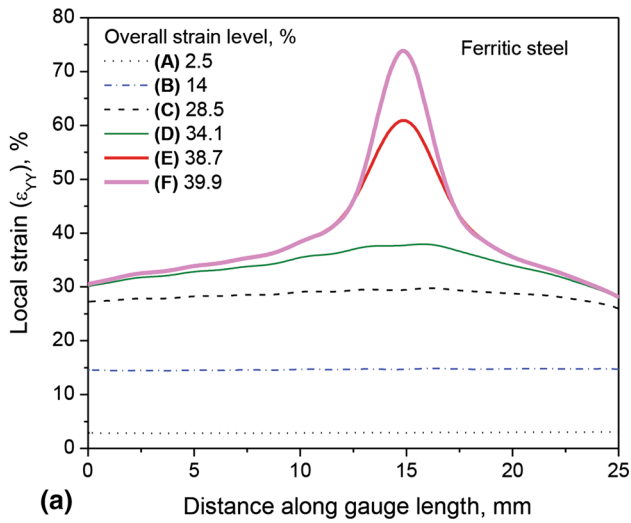


Fig. 6 Evolution of local strain components (ϵ_{XX} and ϵ_{YY}) at various overall strain levels during a tensile test of a ferritic steel (Fig. 5) (a) ϵ_{YY} and (b) ϵ_{XX}

The normal anisotropy coefficient (r) can be defined as the ratio of width strain increment ($d\epsilon_{XX}$) and thickness strain increment ($d\epsilon_{ZZ}$).

$$r = \frac{d\epsilon_{XX}}{d\epsilon_{ZZ}} \quad (\text{Eq 3})$$

We can easily measure $d\epsilon_{XX}$ and $d\epsilon_{ZZ}$ directly from 3D DIC experiment. However, we have used 2D DIC technique. As a result, $d\epsilon_{ZZ}$ can be calculated from volume consistency condition. Considering volume remains constant during the deformation, Eq 4 can be obtained.

$$d\epsilon_{XX} + d\epsilon_{YY} + d\epsilon_{ZZ} = 0 \quad (\text{Eq 4})$$

where $d\epsilon_{XX}$, $d\epsilon_{YY}$ and $d\epsilon_{ZZ}$ are the increment in true strain in the width, axial and thickness directions, respectively.

Thickness direction strain can be obtained by rearranging Eq 4.

$$d\epsilon_{ZZ} = -(d\epsilon_{XX} + d\epsilon_{YY}) \quad (\text{Eq 5})$$

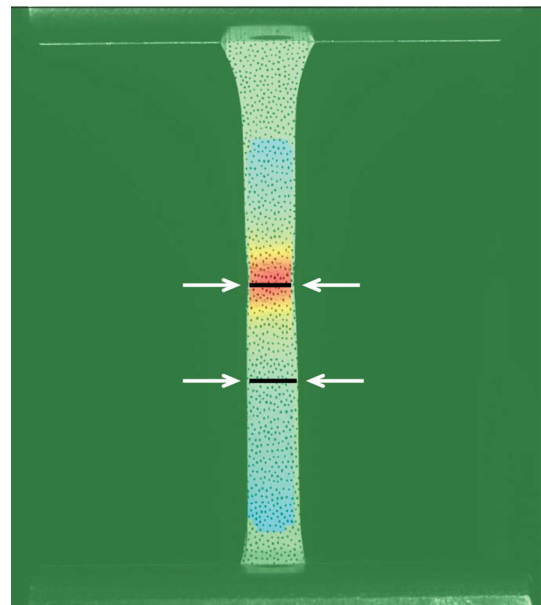


Fig. 7 Horizontal line on the sample surface at necked and outside the necked zone but within the gauge length for investigation of evolution of local strain components (ϵ_{XX} and ϵ_{YY}) at various overall tensile strain levels

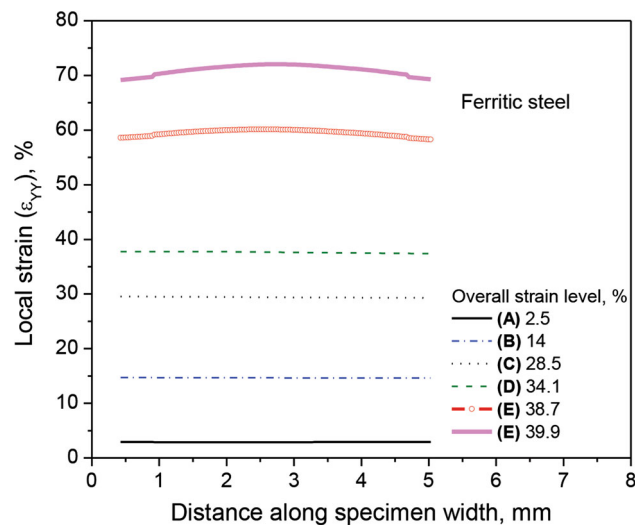


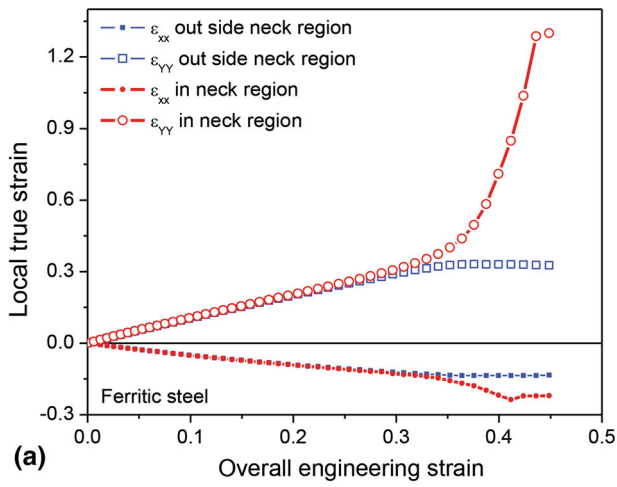
Fig. 8 Evolution of local strain component (ϵ_{YY}) at various overall strain levels during a tensile test of a ferritic steel

So, the normal anisotropy coefficient (r) can be determined from Eq 6.

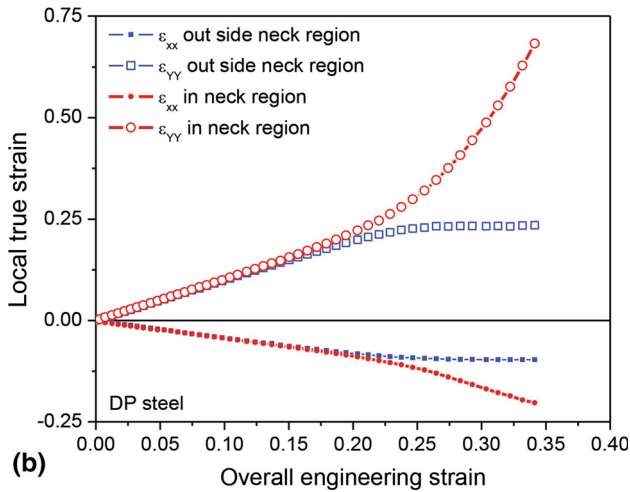
$$r = \frac{d\epsilon_{XX}}{-(d\epsilon_{YY} + d\epsilon_{XX})} \quad (\text{Eq 6})$$

Hill's quadratic normal anisotropic yield criterion is a special case of Hill's general anisotropic yield criterion. In this yield criterion, the equivalent stress (σ_{eq}) is a function of the principal stresses (σ_{YY} and σ_{XX}) and the normal anisotropy coefficient (r). The equivalent stress (σ_{eq}) for plane stress condition can be defined by:

$$\sigma_{eq} = \sqrt{\sigma_{XX}^2 + \sigma_{YY}^2 - \frac{2r}{1+r} \sigma_{XX} \sigma_{YY}} \quad (\text{Eq 7})$$



(a)



(b)

Fig. 9 Evolution of local average strain components (ϵ_{XX} and ϵ_{YY}) at various overall strain levels during a tensile test of a ferritic steel: (a) DP steel and (b) ferritic steel

Similarly the equivalent strain rate ($d\epsilon_{eq}$) can be defined by:

$$d\epsilon_{eq} = \frac{1+r}{\sqrt{1+2r}} \sqrt{d\epsilon_{XX}^2 + d\epsilon_{YY}^2 + \frac{2r}{1+r} d\epsilon_{XX} d\epsilon_{YY}} \quad (\text{Eq 8})$$

The relationship between equivalent stress (σ_{eq}) and major stress (σ_{YY}) can be given as:

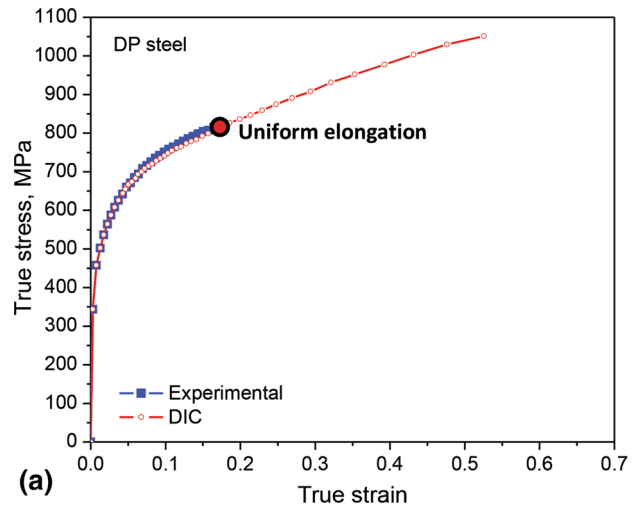
$$\sigma_{eq} = \sigma_{YY} \sqrt{1 + \alpha^2 - \frac{2r}{1+r} \alpha} \quad (\text{Eq 9})$$

Bridgman correction factor (Ref 11) is the ratio of equivalent stress (σ_{eq}) and axial or major stress (σ_{YY}). From Eq 9, instantaneous correction factor can be obtained. Therefore, introduction of separate correction factor for this work is not required. Major stress (σ_{YY}) is the true local average stress along loading direction and can be determined from Eq 10.

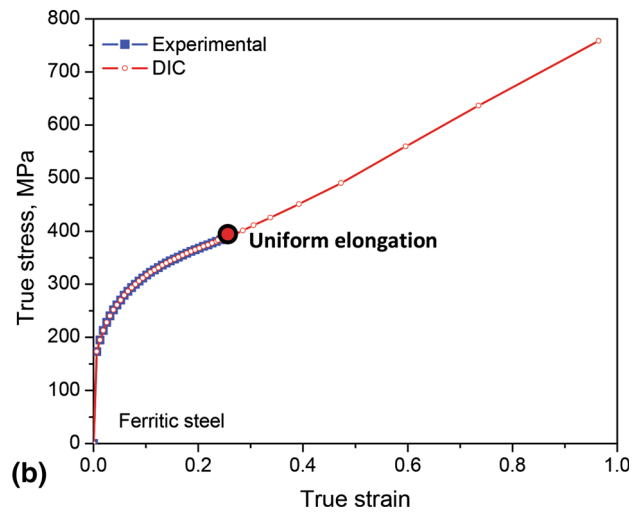
$$\sigma_{YY} = S_{YY} e^{\epsilon_{YY}} \quad (\text{Eq 10})$$

Similarly, the relationship between equivalent strain rate ($d\epsilon_{eq}$) and major strain rate ($d\epsilon_{YY}$) can be given as:

$$d\epsilon_{eq} = d\epsilon_{YY} \frac{1+r}{\sqrt{1+2r}} \sqrt{1 + \beta^2 + \frac{2r}{1+r} \beta} \quad (\text{Eq 11})$$



(a)



(b)

Fig. 10 Comparison of true tensile stress–strain curve of standard tensile test and predicted by DIC with local area correction (a) DP steel and (b) ferritic steel

The relationship between strain rate ratio (β) and stress ratio (α) is:

$$\beta = \frac{(1+r)\alpha - r}{1+r-r\alpha} \quad (\text{Eq 12})$$

And its inverse relationship is:

$$\alpha = \frac{(1+r)\beta + r}{1+r+r\beta} \quad (\text{Eq 13})$$

The steps to determine post-necking stress–strain response of steel sheets are listed in a sequential order:

- i. The true average local strain along the loading direction (ϵ_{YY}) and along the width direction (ϵ_{XX}) in necked zone is directly measured from DIC results.
- ii. Then, the normal anisotropy coefficient (r) can be determined from Eq 6.
- iii. The strain rate ratio (β) can be determined from Eq 1.
- iv. The stress ratio (α) can be determined from Eq 13.
- v. Determine the true stress along loading direction in the necked zone from Eq 10.
- vi. The equivalent stress (σ_{eq}) is determined from Eq 9.

vii. The equivalent strain rate ($d\epsilon_{eq}$) is determined from Eq 11.

Bridgman (Ref 11) corrected local stress and strain state at the necked region because of triaxial stress state presence. In the current work, equivalent stress (Eq 9) and strain (Eq 11) are also determined by introducing correction of local stress and strain state at the necked region.

Based on the above procedure, stress–strain data after necking are calculated and a comparison of true tensile stress–strain curve obtained from standard tensile test and measured by DIC after local stress and strain correction for DP steel and ferritic steel are shown in Fig. 10(a) and (b), respectively.

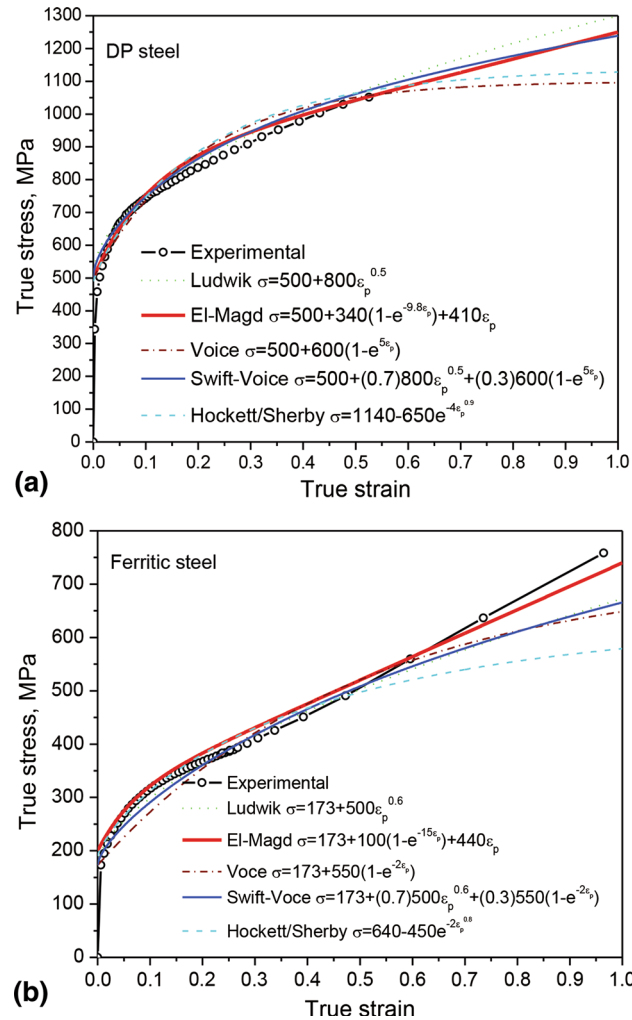


Fig. 11 Fitting of various quasi-static models on true tensile stress–strain curve determined from DIC with local area correction (a) DP steel and (b) ferritic steel

Predictions are found to be in good agreement with the experimental results up to necking/uniform elongation. The nature of the post-necking true tensile stress–strain curve is noted to be in line with the reported results (Ref 2, 6, 7, 10).

To use the post-necking true tensile stress–strain curve accurately in finite element simulation, constitutive description is mandatory. Constitutive relations to describe the quasi-static stress–strain curve of the materials are available in the literature (Ref 26). Some of them are examined in this work to assess their predictive capability in large strain condition. Ludwik (Ref 27) strain hardening law can be expressed by Eq 14.

$$\sigma = \sigma_0 + K\epsilon_p^n \quad (\text{Eq 14})$$

where σ_0 and σ are the yield stress and true stress, ϵ_p is the plastic strain. K and n are material constants for Ludwik law.

El-Magd (Ref 28) strain hardening law can be expressed by Eq 15.

$$\sigma = \sigma_0 + A\epsilon_p + B(1 - e^{-\beta\epsilon_p}) \quad (\text{Eq 15})$$

where A , B and β are the material constant for El-Magd law.

Voce (Ref 29) strain hardening law can be written by Eq 16.

$$\sigma = \sigma_0 + C(1 - e^{-\alpha\epsilon_p}) \quad (\text{Eq 16})$$

where C and α are the material constants for Voce law. Swift-Voce (Ref 30) strain hardening law can be stated as:

$$\sigma = \sigma_0 + zK\epsilon_p^n + (1 - z)C(1 - e^{-\alpha\epsilon_p}) \quad (\text{Eq 17})$$

where z is the material constant. Material constants K and n are same as in Eq 9; similarly, material constants C and α are same as in Eq 16.

Hockett–Sherby (Ref 31) strain hardening law can be stated as:

$$\sigma = F - De^{\lambda\epsilon_p^m} \quad (\text{Eq 18})$$

where F , D , λ and m are material constants for Hockett–Sherby law.

The prediction capabilities of the above constitutive models for large strain deformation are compared in Fig. 11. Material constants for all the models are given in Table 1 for both ferritic and DP steels. Prediction by Swift-Voce and El-Magd laws reasonably matches with experimental results for DP steel (Fig. 11a), while Hockett–Sherby and Voce laws are unable to predict experimental post-necking stress–strain curve accurately. The predictive capability of Ludwik law is also reasonably good for the DP steel. For ferritic steel, prediction of post-necking stress–strain curve by El-Magd law is the best (Fig. 11b), while Hockett–Sherby and Voce laws are unable to predict the experimental results accurately. Swift-Voce and Ludwik laws show average prediction capability of post-necking stress–strain curve for ferritic steel. Considering the prediction capability of all the examined models for both the

Table 1 Material constants for ferritic and DP steels in different models

Steel	σ_0	K	n	A	B	β	C	α	z	F	D	λ	m
DP	500	800	0.5	410	340	9.8	600	5	0.7	1140	650	4	0.9
Ferritic	200	500	0.6	440	100	15	550	2	0.7	640	450	2	0.8

steels, El-Magd law has been found to satisfactorily match the post-necking stress–strain curves in both the cases.

4. Conclusions

An alternative approach to determine post-necking true stress–strain curve of steel sheets experimentally is presented in this work. DIC is used to measure the strain fields on the surface of the specimen with a rectangular cross section in a quasi-static tensile experiment. Local stress and strain corrections in necked zone are done from the experimentally measured local strains at the necked zone and classical theory of plasticity. The proposed approach is validated by the experimental results for ferritic and DP steels. Application of the proposed approach is limited to diffused necking zone. The predictive capabilities of various quasi-static isotropic hardening laws are examined in the post-necking large strain levels. El-Magd law is found to successfully predict the post-necking stress–strain curve for both ferritic and DP steels.

References

1. J. Davis, *Tensile Testing*, 2nd ed., ASM International, Materials Park, OH, 2004
2. A. Nasser, A. Yadav, P. Pathak, and T. Altan, Determination of the Flow Stress of Five AHSS Sheet Materials (DP 600, DP 780, DP780-CR, DP 780-HY and TRIP 780) Using the Uniaxial Tensile and the Biaxial Viscous Pressure Bulge (VPB) Tests, *J. Mater. Process. Technol.*, 2010, **210**, p 429–436
3. V. Tvergaard, Necking in Tensile Bars with Rectangular Cross-section, *Comput. Methods Appl. Mech. Eng.*, 1993, **103**(1), p 273–290
4. I. Scheider, W. Brocks, and A. Corneck, Procedure for the Determination of True Stress–Strain Curves from Tensile Tests with Rectangular Cross-section Specimens, *ASME J. Eng. Mater. Technol.*, 2004, **126**, p 70–76
5. S. Coppiters, S. Cooreman, H. Sol, P. Van Houtte, and D. Debruyne, Identification of the Post-necking Hardening Behaviour of Sheet Metal by Comparison of the Internal and External Work in the Necking Zone, *J. Mater. Process. Technol.*, 2011, **211**, p 545–552
6. N. Tardif and S. Kyriakides, Determination of Anisotropy and Material Hardening for Aluminum Sheet Metal, *Int. J. Solids Struct.*, 2012, **49**(25), p 3496–3506
7. L. Wang and W. Tong, Identification of Post-necking Strain Hardening Behavior of Thin Sheet Metals from Image-Based Surface Strain Data in Uniaxial Tension Tests, *Int. J. Solids Struct.*, 2015, **75–76**, p 12–31
8. K. Zhao, L. Wang, Y. Chang, and J. Yan, Identification of Post-necking Stress–Strain Curve for Sheet Metals by Inverse Method, *Mech. Mater.*, 2016, **92**, p 107–118
9. D. Gerbig, A. Bower, V. Savic, and L.G. Hector, Jr., Coupling Digital Image Correlation and Finite Element Analysis to Determine Constitutive Parameters in Necking Tensile Specimens, *Int. J. Solids Struct.*, 2016, **15**, p 496–509
10. S. Marth, H.-A. Haggblad, M. Oldenburg, and R. Ostlund, Post Necking Characterisation for Sheet Metal Materials Using Full Field Measurement, *J. Mater. Process. Technol.*, 2016, **238**, p 315–324
11. P.W. Bridgman, *Studies in Large Plastic Flow and Fracture*, McGraw Hill, New York, 1952
12. Z.L. Zhang, M. Hauge, J. Odegard, and C. Thaulow, Determining True Stress–Strain Curve from Tensile Specimens with Rectangular Cross-section, *Int. J. Solids Struct.*, 1999, **36**, p 3497–3516
13. P. Koc and B. Štok, Computer-Aided Identification of the Yield Curve of a Sheet Metal After Onset of Necking, *Comput. Mater. Sci.*, 2004, **31**, p 155–168
14. J. Kajberg and G. Lindkvist, Characterisation of Materials Subjected to Large Strains by Inverse Modeling Based on In-Plane Displacement Fields, *Int. J. Solids Struct.*, 2004, **41**, p 3439–3459
15. H. Tao, N. Zhang, and W. Tong, An Iterative Procedure for Determining Effective Stress–Strain Curves of Sheet Metals, *Int. J. Mech. Mater. Des.*, 2009, **5**, p 13–27
16. S. Holmberg, B. Enquist, and P. Thilderkvist, Evaluation of Sheet Metal Formability, *J. Mater. Process. Technol.*, 2004, **145**, p 72–83
17. M. Merklein, J. Lechler, and M. Geigner, Characterisation of the Flow Properties of the Quenchenable Ultra High Strength Steel 22MnB5, *Ann. CIRP*, 2006, **1**, p 229–232
18. M. Grediac and F. Pierron, Applying the Virtual Fields Method to the Identification of Elasto-Plastic Constitutive Parameters, *Int. J. Plast.*, 2006, **22**(4), p 602–627
19. Y. Ling, Uniaxial True Stress–Strain After Necking, *AMP J. Technol.*, 1996, **5**, p 37–48
20. M.S. Joun, J.G. Eom, and M.C. Lee, A New Method for Acquiring True Stress–Strain Curves over a Large Range of Strains Using a Tensile Test and Finite Element Method, *Mech. Mater.*, 2008, **40**(7), p 586–593
21. J.-H. Kim, A. Serpantié, F. Barlat, F. Pierron, and M.-G. Lee, Characterization of the Post-necking Strain Hardening Behavior Using the Virtual Fields Method, *Int. J. Solids Struct.*, 2013, **50**, p 3829–3842
22. M. Dunand and D. Mohr, Hybrid Experimental–Numerical Analysis of Basic Ductile Fracture Experiments for Sheet Metals, *Int. J. Solids Struct.*, 2010, **47**(9), p 1130–1143
23. P.C. Chakraborti and M.K. Mitra, Microstructure and Tensile Properties of High Strength Duplex Ferrite-Martensite (DFM) Steels, *Mater. Sci. Eng. A*, 2007, **466**(1–2), p 123–133
24. LaVision, 2017, <http://www.lavision.de/en/products/strainmaster/strain-master-dic.php>
25. C.C. Tasan, J.P.M. Hoefnagels, and M.G.D. Geers, Identification of the Continuum Damage Parameter: An Experimental Challenge in Modeling Damage Evolution, *Acta Mater.*, 2012, **60**, p 3581–3589
26. S.K. Paul, Predicting the Flow Behavior of Metals Under Different Strain Rate and Temperature Through Phenomenological Modeling, *Comput. Mater. Sci.*, 2012, **65**, p 91–99
27. P. Ludwik, *Element der Technologischen Mechanik*, Springer, Berlin, 1909
28. E. El-Magd and M. Abouridouane, Einfluss der Umformgeschwindigkeit und temperatur auf das Fließverhalten der Magnesiumlegierung AZ80, *Z. Metallk.*, 2001, **92-1**, p 1231–1235
29. E. Voce, The Relationship Between Stress and Strain for Homogeneous Deformation, *J. Inst. Met.*, 1948, **74**, p 537–562
30. J.H. Sung, J.H. Kim, and R.H. Wagoner, A Plastic Constitutive Equation Incorporating Strain, Strain-Rate, and Temperature, *Int. J. Plast.*, 2010, **26**, p 1746–1771
31. J.E. Hockett and O.D. Sherby, Large Strain Deformation of Polycrystalline Metals at Low Homologous Temperatures, *J. Mech. Phys. Solid*, 1975, **23-2**, p 87–98